Analytica Chimica Acta 1182 (2021) 338939

Contents lists available at ScienceDirect

Analytica Chimica Acta

journal homepage: www.elsevier.com/locate/aca

Colorimetric and electrochemical detection of SARS-CoV-2 spike antigen with a gold nanoparticle-based biosensor

Erman Karakuş [a, *], Eda Erdemir [a], Nisa Demirbilek [a], Lokman Liv [b]

[a] Organic Chemistry Laboratory, Chemistry Group, The Scientific and Technological Research Council of Turkey, National Metrology Institute, (TUBITAK UME), 41470, Gebze, Kocaeli, Turkey
[b] Electrochemistry Laboratory, Chemistry Group, The Scientific and Technological Research Council of Turkey National Metrology Institute, (TUBITAK UME), 41470, Gebze, Kocaeli, Turkey

HIGHLIGHTS

- The developed probe (**AuNP-mAb**) exhibits dual sensing mode for the detection of SARS-CoV-2 spike antigen (S-Ag).
- **AuNP-mAb** allows viusal detection (colorimetric) of S-Ag with a detection limit of 48 ng/mL.
- Electrochemical detection of S-Ag is achieved by a disposable screen-printed gold electrode with a detection limit of 1 pg/mL.
- Neither method exhibits cross-reactivity with other viral proteins such as Influenza A, MERS-CoV and Streptococcus pneumoniae.
- **AuNP-mAb** allows simple and rapid analysis of S-Ag in saliva sample.

GRAPHICAL ABSTRACT

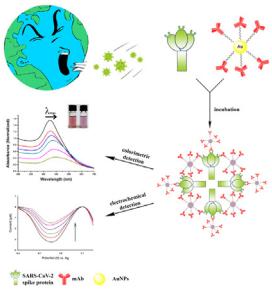

ARTICLE INFO

Article history:
Received 7 May 2021
Received in revised form
9 August 2021
Accepted 10 August 2021
Available online 11 August 2021

Keywords:
COVID-19
SARS-CoV-2
Colorimetric biosensor
Electrochemical biosensor
Gold nanoparticles
Dual-sensing probe

ABSTRACT

Since emerging in China in December 2019, COVID-19 has spread globally, wreaked havoc for public health and economies worldwide and, given the high infectivity and unexpectedly rapid spread of the virus responsible—that is, severe acute respiratory syndrome coronavirus 2 (SARS-CoV-2)—urged the World Health Organization to declare it a pandemic. In response, reducing the virus's adverse effects requires developing methods of early diagnosis that are reliable, are inexpensive and offer rapid response. As demonstrated in this article, the colorimetric and electrochemical detection of SARS-CoV-2 spike antigen with gold nanoparticle-based biosensors may be one such method. In the presence of the SARS-CoV-2 spike antigen, gold nanoparticles aggregated rapidly and irreversibly due to antibody −antigen interaction and consequently changed in colour from red to purple, as easily observable with the naked eye or UV−Vis spectrometry by way of spectral redshifting with a detection limit of 48 ng/mL. Moreover, electrochemical detection was achieved by dropping developed probe solution onto the commercially available and disposable screen-printed gold electrode without requiring any electrode preparation and modification. The method identified 1 pg/mL of the SARS-CoV-2 spike antigen and showed a linear response to the SARS-CoV-2 spike antigen ranging from 1 pg/mL to 10 ng/mL. Both

* Corresponding author.
E-mail address: erman.karakus@tubitak.gov.tr (E. Karakuş).

https://doi.org/10.1016/j.aca.2021.338939

methods were highly specific to detecting the SARS-CoV-2 spike antigen but not other antigens, including influenza A (i.e. H1N1), MERS-CoV and *Streptococcus pneumoniae*, even at high concentrations.

1. Introduction

Since emerging in December 2019 in Wuhan, the capital of China's Hubei Province, the unprecedented coronavirus 2019 (COVID-19) has caused massive disruptions for public health and economies worldwide [1–4]. Known to be caused in humans by respiratory infections of the severe acute respiratory syndrome coronavirus 2 (SARS-CoV-2), COVID-19's high infectivity and rapid spread have posed serious threats across the globe, as evidenced by the steep rise in mortality in the past 18 months, during which time more than 4.2 million people have died worldwide [5,6].

On 31 January 2020, the World Health Organization listed COVID-19 as a "Public Health Emergency of International Concern" [1]. The disease's well-known symptoms usually begin with a fever and difficulty with breathing, followed by a severe cough and other acute symptoms, and may even result in death [7,8]. However, asymptomatic cases have also been reported [9,10]. With or without symptoms, the dramatic increase in the number of cases of COVID-19 has driven high demand for diagnostic tests to confirm the virus's presence rapidly, accurately and selectively [11–14]. To date, the process of developing such tests has confirmed that spike (S), envelope (E), membrane (M) and nucleocapsid (N) are the significant structural proteins for coronavirus particles [15]. Added to that evidence, various studies have indicated that the spike protein plays the most important role in the virus's entry and binding to the human angiotensin-converting enzyme 2 (ACE2) receptor on the surface of cells, and the spike protein has thus become a promising new target for sensors [16–20]. Accordingly, various methods have been developed for the detection of COVID-19 such as virus nucleic acid real time-PCR (RT-PCR) [21–23], CT imaging [24], enzyme-linked immunosorbent assay (i.e. ELISA) [25], point-of-care tests [26], lateral flow immunoassay tests [25,27,28] and tests for some haematological parameters [29].

Although those methods afford considerable convenience in detecting SARS-CoV-2 and diagnosing COVID-19 and its progression, most of them share certain limitations. For example, the most commonly used and arguably most reliable method, reverse transcription RT-PCR, which can detect viral genetic material (i.e. RNA) in samples collected with nasopharyngeal swabs, its administration requires highly trained personnel, which prevents its general application and use. It is also a time-consuming method, one entailing long nucleic acid extraction, and has been prone to giving false negatives [30]. Given such limitations in the most frequently used, reliable method, a much simpler, faster, more sensitive method has been needed to detect SARS-CoV-2, provide timely treatment to patients and prevent the spread of the disease. Therefore there is a continuous demand for selective, rapid, repeatable, cost-effective, ready-to-use, and ultrasensitive biosensors. Against that background, the demand for rapid, selective, repeatable, cost-effective, ready-to-use, ultrasensitive biosensors has continually risen. Of the numerous biosensors using colorimetric [31–34], scanometric [35], electrochemical [36,37], and fluorometric [38,39] systems to detect well-known human viruses [40–42], colorimetric assay is a simple, direct method of visual detection that does not require any complicated equipment. Metal nanoparticle-based colorimetric assays are commonly used to diagnose diseases in humans, and the development of those biosensors has also enabled the development of rapid colorimetric diagnostic tests that can be used even at home. In particular, gold nanoparticles (AuNPs) are often used in colorimetric assays due to their easy synthesis, low cost, simplicity, practicality, unique optical properties and the functionality of their surfaces [43–47]. Colorimetric detection based on AuNPs takes advantage of the change in colour, from red to purple, that occurs in a colloidal suspension via antigen–antibody interaction [48,49]. In parallel, electrochemical sensing methods of detecting proteins, nucleic acids, bacteria, viruses, antibodies and their fragments have also become attractive owing to their simplicity, low cost, rapidity, high sensitivity and selectivity [37,50–53]. Due to those combined advantages, electrochemical and colorimetric biosensors and/or methods could be developed to determine molecular SARS-CoV-2 antigens, antibodies and/or their fragments. Indeed, in the past few months alone, several nanoscale integrated structures based on optical and electronic systems have been reportedly been able to detect the SARS-CoV-2 spike protein with high sensitivity [54–68].

In this article, we present the design, synthesis and spectral features of an AuNP-based biosensor platform for detecting the SARS-CoV-2 spike antigen with high selectivity and sensitivity. The detection process relies on two techniques: a voltammetric method and an optical sensing method using the naked eye or UV–Vis spectrophotometry.

2. Methods

2.1. Materials

Gold (III) chloride trihydrate ($HAuCl_4$, ≥99.9, Sigma-Aldrich 520918), 11-mercaptoundecanoid acid (MUA, ≥95, Sigma-Aldrich 450561), Sodium citrate dihydrate (≥99, Sigma-Aldrich W302600) N-(3-Dimethylaminopropyl)-N′-ethylcarbodiimide hydrochloride (EDC, ≥98, Sigma-Aldrich 03450), N-Hydroxysuccinimide (NHS, 98%, Sigma-Aldrich 130672), Potassium phosphate monobasic solution (KH_2PO_4, reagent grade 1.0 M, Sigma-Aldrich P8709), Bovine serum albumin (BSA, ≥98, Sigma-Aldrich 05470), Tween 20 (BioXtra, Sigma-Aldrich P7949) and other chemicals were purchased from Sigma-Aldrich and used without further purification. SARS-CoV-2 spike monoclonal antibody (mAb) (Chimeric MAb Cat: 40150-D00), SARS-CoV-2 (2019-nCoV) spike S1-his recombinant protein (HPLC-verified, Cat: 40591-V08H), MERS-CoV spike/S1 protein (S1 Subunit, aa 1–725, His Tag, Cat: 40069-V08B1), Influenza A H1N1Hemagglutin/H0A protein (Cat: 11055-VNAB) were obtained from Sino Biological. *Streptococcus pneumoniae* antigen, the native extract was purchased from Native Antigen Company. Ultrapure water was procured from Milli-Q Direct 8 system. All the antibody and antigen solutions were prepared in phosphate buffer solution (pH = 7.4) and stored in protein LoBind Eppendorf tubes.

2.2. Instruments

A UV-1900i spectrophotometer (Shimadzu) and quartz micro cuvettes (700 μL, Hellma) were used for all local surface plasmon resonance (LSPR) analyses. The LSPR band of AuNPs and functionalised AuNPs were monitored between 300 and 800 nm in order to

track alterations in the size and distribution of particles. The hydrated particle sizes were evaluated using a Zetasizer with dynamic light scattering (DLS; Malvern Zetasizer Nano ZS-3600), while the surface functionalisation of AuNPs was investigated with a Bruker Alpha II compact Fourier Transform Infrared (FTIR) spectrometer. High-resolution transmission electron microscopy (TEM) was performed with a JEOL JEM 2100 HRTEM at 200 kV to characterise the morphologies of monodispersed AuNPs and AuNPs bioconjugates before and after incubation with the SARS-CoV-2 spike antigen. Images were taken with a Gatan Model 833 Orius SC200D CCD camera, and carbon support film-coated copper TEM grids (Electron Microscopy Sciences, CF200–Cu, 200 mesh) were used. All incubations were performed in a MTC-100 Miulab thermoshaker, and a Mettler Toledo Seven Compact pH meter with InLab Expert Pro-ISM combined with a pH electrode was used to prepare the buffer solutions. Electrochemical measurements were taken with a Metrohm Dropsens potentiostat–galvanostat, a Dropsens boxed connector (DSC4MM) and a screen-printed gold electrode (Dropsens C220BT) consisting of working gold and auxiliary electrodes and a silver reference electrode at 21 ± 3 °C and 45 ± 15% relative humidity.

2.3. Preparation of AuNPs

AuNPs were synthesised by following a citrate reduction method [69]. First, all glassware used in the experiment was thoroughly cleaned with aqua regia (3:1 (v/v) HCl:HNO_3), rinsed with deionised water and oven-dried before use. Briefly, an aqueous solution of 2.5 mL of 5 mM $HAuCl_4$ was added to 50 mL of ultrapure water under vigorous stirring until boiling. After boiling, 1% sodium citrate solution was rapidly added to the solution, which was then boiled for another 10 min under vigorous stirring, during which time the solution's colour changed from pale yellow to bright red. After the solution cooled naturally for another 10 min under constant stirring, the resulting colloidal gold solutions were filtered through a 0.45-μm membrane and stored in the dark at 4 °C until use. As the value of the extinction coefficient for the AuNPs with a diameter of 15 nm is 3.6×10^8 cm^{-1} M^{-1} [62], the concentration of the AuNPs with the approximate diameter of 15 nm was estimated to be 2.4 nM.

2.4. Surface modification of AuNPs

The citrate groups on the surface of the AuNPs were exchanged with 11-mercaptoundecanoic acid (MUA) following slight modifications made according to the literature [47]. A schematic illustration of the process appears in Scheme 1. Briefly put, 100 μL of ethanolic solution containing MUA (10 mM) was added to 1 mL of citrate-capped solution with AuNPs, and the reaction mixture was incubated overnight at room temperature before centrifugation. The final mixture was centrifuged at 13,200 rounds of per minute (rpm) for 15 min, washed twice with phosphate buffer (PB, 10 mM, pH 7.4) to remove unbound MUA molecules and resuspended in PB (10 mM, pH 7.4) containing 0.2 mg/mL of Tween 20. The carboxylic groups of linkers were activated in a freshly prepared solution of 5 mM of EDC and 7.5 mM of NHS. The AuNPs were reacted with 20 μL of the EDC–NHS mixture with gentle shaking for 0.5 h at room temperature, which ultimately yielded NHS-terminated AuNPs (**AuNPs**–**MUA**).

2.5. Preparation of AuNPs–mAb

The conjugate of **AuNPs**–**mAb** was prepared by adding 1.5 μg of the SARS-CoV-2 spike antibody (mAb) to 1 mL of activated AuNPs (**AuNPs**–**MUA),** followed by incubation at 37 °C for 1 h with gentle shaking at 200 rpm, during which time the mAb was reacted with AuNPs through covalent bond formation via EDC–NHS cross-linking agents. After being blocked by 10 μL of 1% (m/v) BSA in 10 mM PB for 15 min at 37 °C, the **AuNPs**–**mAb** was centrifuged for 15 min at 13,200 rpm at 4 °C to remove the unbound protein. The supernatant was discarded, and the sediment was washed twice with PB (10 mM, pH 7.4) containing 0.2 mg/mL of Tween 20. Last, the **AuNPs**–**mAb** conjugate was resuspended in PB and stored at 4 °C for subsequent experiments.

2.6. Detection of the recombinant SARS-CoV-2 spike antigen based on LSPR

The SARS-CoV-2 spike antigen was diluted serially at 250, 500, 750, 1000, and 2000 ng mL^{-1}, and the proper amount was added to one-fold-concentrated **AuNPs**–**mAb** conjugate solution, followed by incubation at room temperature for 10 min. The colour of the mixtures changed from red to purple, and the SARS-CoV-2 spike antigen could be detected with the naked eye and based on LSPR with redshifting (~25 nm).

2.7. Detection of the recombinant SARS-CoV-2 spike antigen based on the electrochemical method

Square wave voltammetry (SWV) was performed with 5 mV of step potential, 20 mV of pulse amplitude, a frequency of 10 Hz and a scan rate of 50 mV/s. Cyclic voltammetry (CV) was performed with 2.5 mV of step potential and a scan rate of 50 mV/s. Both SWV and CV measurements were performed with 50 μL of **AuNPs**–**mAb** in PB solution (10 mM, pH 7.4) containing 0.2 mg/mL of Tween 20 and with a proper amount of the SARS-CoV-2 spike antigen (1, 10, 100,

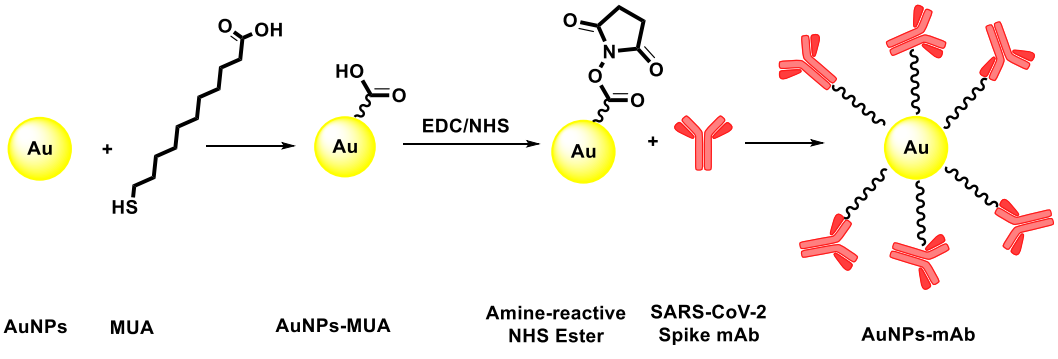

Scheme 1. Schematic illustration of the formation of **AuNP**–**mAb** conjugates.

10^3 and 10^4 pg mL^{-1}) by using a commercially available screen-printed gold electrode as a supporting surface. After each measurement, the sensor was washed with ethanol, dried with argon gas and filled with 50 μL of the new solution.

2.8. Sample preparation

Saliva samples were collected from six healthy individuals and half of the samples were spiked with 500 ng/mL and 10 pg/mL of the SARS-CoV-2 spike antigen for optical and electrochemical measurements, respectively. Then, all of the samples were transferred into the **AuNPs–mAb** in PB solution (10 mM, pH 7.4) containing 0.2 mg/mL of Tween 20. The standard measurement procedure (explained in Section 2.6 and 2.7) was performed for both methods and analysed using external calibration curve.

3. Result and discussion

3.1. Synthesis and characterisation of AuNPs

Size-controlled AuNPs were obtained by way of citrate reduction. Usually, AuNPs interact with each other via Van der Waals forces at short distances; negatively charged citrate ions on the surface of AuNPs provide electrostatic repulsion, which repels AuNPs and precludes them from aggregating. In our research, the size of synthesised AuNPs was determined by DLS and TEM as 16 nm and thus similar to reports in the literature [70]. TEM images revealed that AuNPs exhibited good monodispersity, were similar in size and low aspect ratio. The characteristic absorption peak was seen at 520 nm on the UV–Vis spectrum, with the narrow spectral bandwidth showing the monodispersity of the AuNPs as well (Fig. 1).

To measure DLS, we prepared the solution of AuNPs in distilled water, not in a buffer solution such as PB, PBS and HEPES, which can reduce the repulsion of AuNPs and risks their aggregation. DLS revealed that the average size of AuNPs was 16 nm (range: 11.2–20.6 nm), as depicted in Fig. S1. Adding MUA provided a self-assembled monolayer on the gold surface by way of thiol groups, because the MUA linker replaced the citrate molecules and the –SH end of MUA became bound to the surface of AuNPs, the latter of which provided stability. In the process, the long alkyl chain supplied elasticity such that the active site of the linker could easily interact with different types of ligands. Among the results, the UV–Vis spectrum of the MUA-linked AuNPs exhibited a moderate shift in the LSPR peak from 520 to 523 nm, as previously described in the literature [47] and the spectrum showed a single narrow LSPR peak without broadening, which confirms that AuNPs do not aggregate due to the chemisorption of the MUA linker. FTIR analysis, performed to ensure ligand exchange on the surface of the AuNPs, revealed a broad peak at 3200 cm^{-1}; such peak refers to O–H stretching vibrations that can relate to trace water due to insufficient drying. The presence of the sharp, strong peaks at 2915 and 2848 cm^{-1} for pure MUA are attributable to the symmetric and asymmetric stretching of the CH_2 groups, respectively. In the case of **AuNPs–MUA**, the peaks remained visible, which confirms the success of ligand exchange (Fig. S2). Because the **AuNP–MUA** complex was activated by EDC–NHS coupling, the efficiency of which was usually low and sensitive to pH, we used Tween 20 in buffer solution (pH = 7.4) to maintain stability. When Tween 20 was not introduced, by contrast, AuNPs aggregated irreversibly. We also tested the stability of the AuNPs and the coupling process in water, PBS (10 mM), PB (10 mM) and HEPES (10 mM) buffers by comparing their LSPR peaks. PB buffer (10 mM) was chosen as the most suitable buffer for both AuNPs and the coupling process without proceeding with any aggregation (data not shown). Thus, we used 10 mM of PB with Tween 20 (0.2 mg/mL) as a buffer for all experiments reported here.

After the activation of **AuNPs–MUA** with EDC–NHS, 1.5 μg/mL of the SARS-CoV-2 spike antibody (mAb) was introduced to the activated complex to obtain covalent bonding between the antibody's amine groups and complex's carboxylate groups. An optimisation study was performed to determine the ideal concentration of mAb by experimenting with different amounts of mAb (0.5, 1.0, 1.5, 2.0 and 3.0 μg/mL), for results indicating any increment of antigen capture efficiency exceeding 1.5 μg/mL of mAb. Thus, the optimal concentration of mAb was determined to be 1.5 μg/mL (Fig. S3). **AuNPs–mAb** exhibited a 3nm shift (526 nm) in the UV–Vis spectrum (Fig. 2). On top of that, the conjugate preserved its red colour and was highly stable in the solution containing 0.1 M of NaCl.

3.2. Colorimetric detection of the SARS-CoV-2 spike antigen with the AuNP–mAb probe

Under optimised conditions, we investigated the ability of the **AuNPs-mAb** probe to detect the SARS-CoV-2 spike antigen using

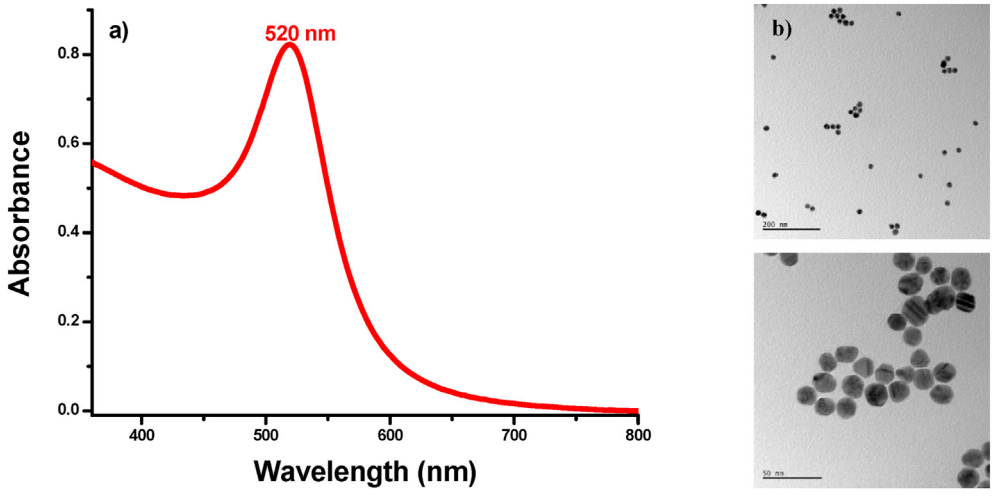

Fig. 1. **(a)** UV–Vis spectrum of the AuNPs. **(b)** TEM images of the AuNPs indicating the size and distribution at different magnifications. Scale bar: 200 nm and 50 nm.

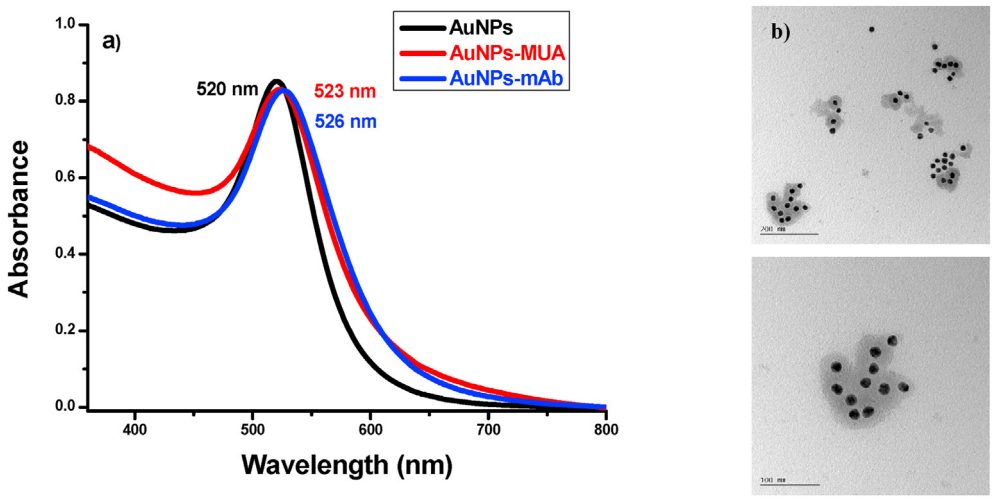

Fig. 2. **(a)** UV–Vis spectrum indicating the absorbance of the modification of AuNPs (black line), MUA (red line) and **AuNPs–mAb** (blue line). **(b)** TEM images of **AuNPs–mAb** indicating the size and distribution at different magnifications. Scale bar: 200 nm and 100 nm. (For interpretation of the references to color in this figure legend, the reader is referred to the Web version of this article.)

LSPR. To obtain good capture efficiency, 200 μL of the **AuNP–mAb** probe was incubated with different amounts of the SARS-CoV-2 spike antigen for 10 min at room temperature. In the presence of the spike antigen (2 μg/mL), **AuNPs–mAb** bound with the antigen particles, thereby providing an agglomeration of AuNPs with both spectral redshift (~25 nm) and a change in colour visible with the naked eye (Fig. 3a). Moreover, TEM images clearly showed that the **AuNP–mAb** probes were attached to the surface of the antigen particles. DLS analysis revealed that the hydrated particle size of the **AuNPs–mAb** increased from 34 nm to 264 nm after the addition of the SARS-CoV-2 spike antigen. The results thus indicated that method can be used to detect the SARS-CoV-2 spike antigen (Fig. S1).

The mechanism of **AuNPs–mAb** based detection of SARS-CoV-2 spike antigen was shown in Scheme 2. Conjugated gold nanoparticles with monoclonal SARS-CoV-2 spike antibody which is highly specific to SARS-CoV-2 spike antigen. **AuNPs–mAb** probe can be specifically arranged and lead to networking on the SARS-CoV-2 spike antigen surface which reduces the distance between each AuNPs and aggregation occurs. In this case, this aggregation of the **AuNPs–mAb** probe causes slight increase the size of the particles and such event produces redshift and broadening as well as decreasing LSPR peak in the spectrum. Decreasing the peak intensity can be explained that the size and amount of SARS-CoV-2 spike antigen are larger than **AuNPs–mAb** (34 nm) and some of **AuNPs–mAb** are bounded to antigen surface which results fall in absorbance peak. It should be mentioned that absorbance value only diminished after the recognition event between **AuNPs–mAb** and SARS-CoV-2 spike antigen.

3.3. *Sensitivity of the detection of the SARS-CoV-2 spike antigen based on LSPR*

The sensitivity of our probe was examined by measuring absorbance versus increasing amounts of the SARS-CoV-2 spike antigen. The first signal change occurred with the addition of 250 ng/mL of the antigen, which caused a redshift in the LSPR peak of the **AuNP–mAb** probe from 526 nm to 528 nm (Fig. 4a). The linear relationship was observed between λ_{max} and the SARS-CoV-2 spike antigen concentration, for a correlation coefficient of 0.99

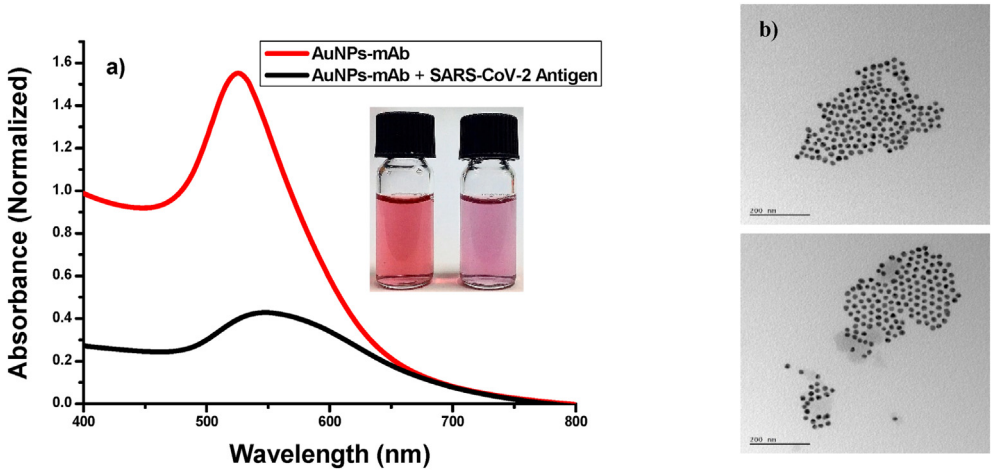

Fig. 3. **(a)** Absorption spectra of **AuNPs–mAb** in the absence (red line) and presence (black line) of 2 μg/mL of the SARS-CoV-2 spike antigen. **(b)** TEM images of **AuNPs–mAb** after incubation with the SARS-CoV-2 spike antigen. Scale bar: 200 nm. (For interpretation of the references to color in this figure legend, the reader is referred to the Web version of this article.)

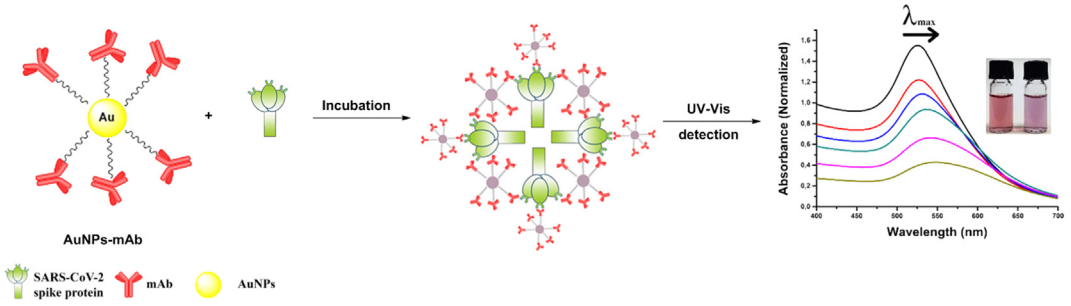

Scheme 2. UV–vis detection of SARS-CoV-2 spike antigen based on the aggregation of **AuNPs**–**mAb** on the SARS-CoV-2 spike antigen surface.

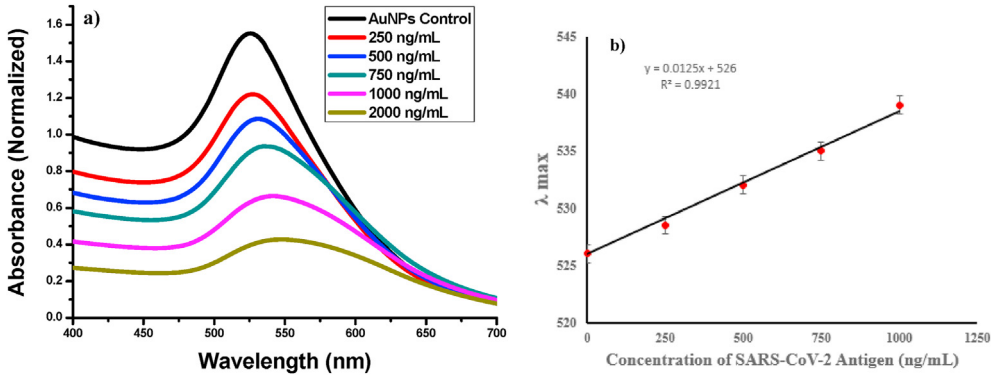

Fig. 4. **(a)** UV–Vis spectrum of **AuNPs**–**mAb** in response to different amounts of the SARS-CoV-2 spike antigen (i.e. 250, 500, 750, 1000 and 2000 ng/mL). **(b)** Redshifted wavelength of LSPR's peak in the presence of different amounts of the SARS-CoV-2 spike antigen (i.e. 250, 500, 750 and 1000 ng/mL).

that shows the method's applicability in quantitative analysis. The limit of detection was calculated with $3s_{y/x}/m$ equation where $s_{y/x}$ is the residual standard error obtained from calibration graph data by regression analysis and m is the slope of calibration curve as 48 ng/mL.

3.4. Selectivity and stability of SARS-CoV-2 spike antigen detection based on LSPR

Because selectivity is a crucial parameter for detection, the selectivity of our **AuNP**–**mAb** probe was tested with different types of spike antigens, including the influenza A antigen (i.e. H1N1), the MERS-CoV antigen and the *Streptococcus pneumoniae* antigen. Other antigens were added to our probe solution in a concentration of 1 μg/mL under the same and optimised conditions. The results showed no significant shift in the samples containing other antigens (Fig. 5a). To clarify the probe's storage stability for other applications, the same sample and patch of the **AuNP-mAb** probe in buffer solution (PB pH = 7.4 with 0.2 mg/mL Tween 20) was left at 4 °C in the dark for the different period. After that period, the sample was incubated with 500 ng/mL of the SARS-CoV-2 antigen. Results showed nearly the same signal change after storage for 4 weeks, which suggests that our **AuNP**–**mAb** probe showed good, relatively long-term stability (Fig. 5b).

3.5. Electrochemical detection of the SARS-CoV-2 spike antigen with the AuNP–mAb probe

Because our **AuNPs**–**mAb** probe may have possessed an oxidation–reduction site, it was worth studying the

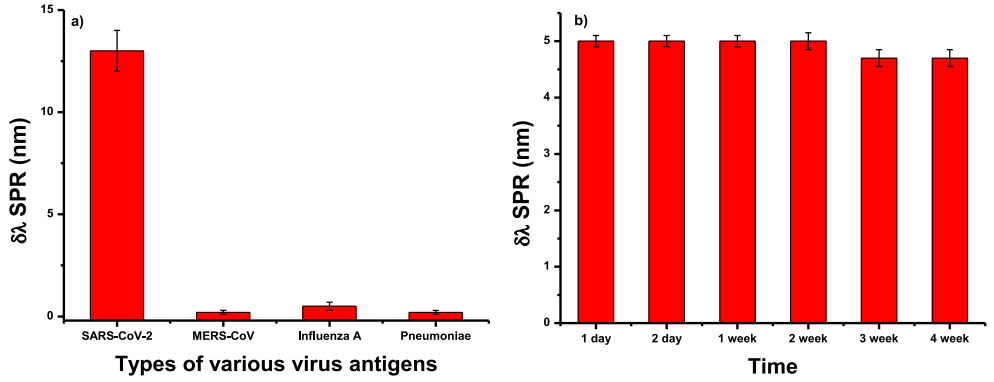

Fig. 5. **(a)** Selectivity of the **AuNP**–**mAb** probe in response to different spike antigens (1 μg/mL) depending on changes in LSPR. **(b)** Stability of the **AuNP**–**mAb** probe in detecting the SARS-CoV-2 spike antigen (500 ng/mL) during different periods.

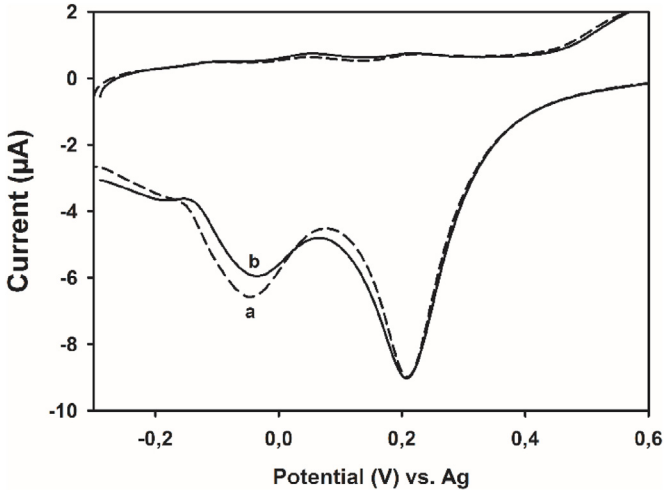

Fig. 6. CVs of **(a) AuNPs-mAb (b)** with 100 ng/mL SARS-CoV-2 spike antigen in 10 mM PB solution (pH = 7.4) with 0.2 mg/mL Tween 20.

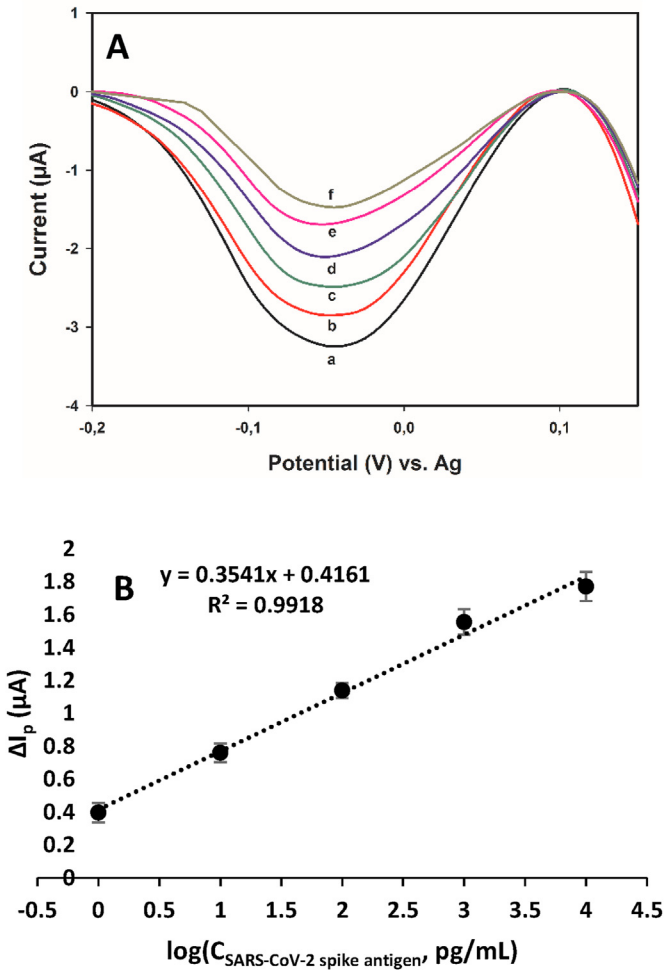

Fig. 7. (A) The square wave voltammograms and **(B)** the calibration curve for SARS-CoV-2 spike antigen **(a)** 10 mM PB solution (pH = 7.4) with 0.2 mg/mL Tween 20, **(b)** + 1 pg/mL, **(c)** + 10 pg/mL, **(d)** + 100 pg/mL, **(e)** + 1 ng/mL and **(f)** + 10 ng/mL of the SARS-CoV-2 spike antigen, respectively. **ΔI_p**: (The reduction signal of **AuNP–mAb**) - (the reduction signal of the added amount of SARS-CoV-2 spike antigen with **AuNP–mAb**).

electrochemistry of the interaction of **AuNPs–mAb** with the SARS-CoV-2 spike antigen. The commercially available and disposable screen-printed gold electrode was used without following any sensor modification and production steps that offers a simple and cheap measurement method. Since screen-printed gold electrode was used, a specific interaction occurred between the gold surface (partially negative charge) and gold particles (partially positive charge) in **AuNPs–mAb**. With the help of a cathodic scan, **AuNPs–mAb** behaved as an electrode material. During the cathodic scan, the groups containing heteroatoms like carbonyl on the surface of **mAb** were reduced. After an increasing amount of SARS-CoV-2 spike antigen addition, antigen-antibody interactions took place in which the signal of the developed sensor decreased due to the lowering free groups including heteroatoms on the surface of mAb. As anticipated, **AuNPs–mAb** had few oxidation peaks but two well-defined reduction peaks at 205 mV and −50 mV (Fig. 6). In particular, the peak at −50 mV decreased with the addition of the SARS-CoV-2 spike antigen.

The sensitivity of the electrochemical system was also examined, as previously done for the colorimetric detection of the SARS-CoV-2 spike antigen. The calibration voltammograms and curve belonging to the SARS-CoV-2 antigen are shown in Fig. 7. The proposed method is able to detect 1 pg/mL of the SARS-CoV-2 spike antigen and has a linear response to the antigen between 1 pg/mL and 10 ng/mL in 10 mM of PB solution (pH = 7.4) containing 0.2 mg/mL of Tween 20.

Using the same strategy, we proceeded with examining selectivity under the same and optimised conditions. The effects of interference with the *Streptococcus pneumoniae*, influenza A and MERS-CoV spike antigens were investigated to evaluate the proposed method's selectivity (Fig. 8). Both the immobilising tendency of the interference on the **AuNP–mAb** probe and the effects of disrupting the binding between the SARS-CoV-2 antibody and antigen were examined, as shown in Fig. 8 and S4, respectively. Ultimately, the proposed electrochemical detection method based on **AuNPs–mAb** showed no response to 100 pg/mL of the interference,

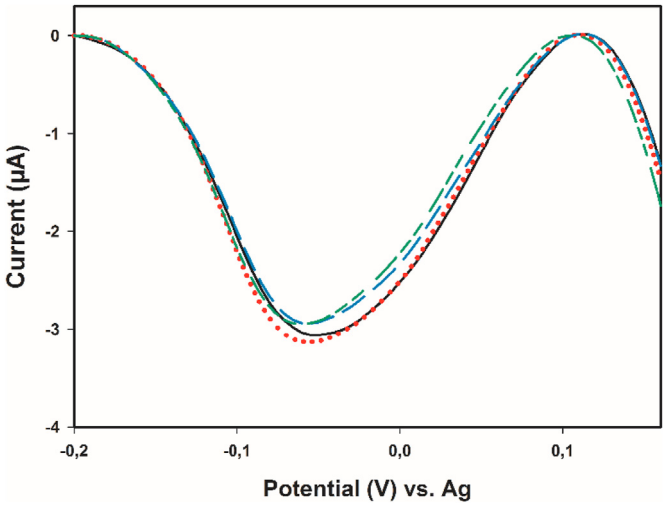

Fig. 8. The immobilisation tendency of the *Streptococcus pneumoniae*, Influenza A and MERS-CoV spike antigens onto **AuNPs-mAb** in 10 mM PB solution (pH = 7.4) with 0.2 mg/mL Tween 20 straight black line: **AuNPs-mAb**, dotted red line: **AuNPs-mAb** + 100 pg/mL *Streptococcus pneumoniae* antigen, dashed blue line: **AuNPs-mAb** + 100 pg/mL Influenza A antigen and mixed-dashed green line: **AuNPs-mAb** + 100 pg/mL MERS-CoV antigen. (For interpretation of the references to color in this figure legend, the reader is referred to the Web version of this article.)

Table 1
The results of spiked saliva samples (n = 6).

Saliva Samples	Added amount of SARS-CoV-2 spike antigen	SARS-CoV-2 spike antigen found (mean ± standard deviation)	Recovery (%) (mean ± standard deviation)	RSD (%)
Optical Method	500 ng mL^{-1}	471.0 ± 10.4 ng mL^{-1}	94.1 ± 2.1	2.2
Electrochemical Method	10 pg mL^{-1}	10.2 ± 0.5 pg mL^{-1}	102.2 ± 4.9	4.8

which was 100-fold relative to the SARS-CoV-2 spike antigen. Those results clearly indicate the satisfactory selectivity of the proposed sensing method. As given in Table S1, **AuNPs−mAb** exhibited comparative advantages over other published studies previously in terms of diversity of the sensing methods and detection limit (Table S1).

3.6. Sample application

When the developed method was applied to the spiked saliva samples to determine the SARS-CoV-2 spike antigen, the relative standard deviation and recovery values for both optical and electrochemical methods varied from 2.2% to 4.8% and 94.1%−102.2%, respectively (Table 1). Absorbance spectra and voltammograms for the spiked and non-spiked saliva samples appear in Fig. S5. The graphs exhibited that our sensing media (**AuNPs-mAb**) was not affected by the saliva matrix. The results generally suggest that the method offers good precision and trueness, thus a good accuracy.

4. Conclusion

In sum, we have developed a simple, rapid (i.e. 10 min), selective, dual-response colloidal AuNP-based biosensing platform that allows both the colorimetric and electrochemical detection of the SARS-CoV-2 spike antigen at the level of ng/mL (i.e. for the colorimetric method) and pg/mL (i.e. for the electrochemical method). The colorimetric method's applicability was confirmed with positive results visible to the naked eye without requiring any sophisticated instruments. Beyond that, the sensor in the developed electrochemical method, as a disposable material, can be reused and does not require time-consuming steps such as sensor preparation and replacement. Moreover, to the best of our knowledge, it is the first electrochemical study for the detection of SARS-CoV-2 spike antigen without requiring a sensor preparation and modification. The developed system is used to detect the SARS-CoV-2 spike antigen in saliva samples successfully and also it offers simplicity, cost-efficiency and speed. Last, neither method exhibits cross-reactivity with other viral proteins (i.e. influenza A, MERS-CoV and *Streptococcus pneumoniae*). Therefore, the biosensing platform can be easily integrated into a ready-to-use commercial kit and adapted for the diagnosis of other emerging viral diseases.

CRediT authorship contribution statement

Erman Karakuş: Conceptualization, Methodology, Formal analysis, Writing − original draft, Writing − review & editing. **Eda Erdemir:** Formal analysis, Investigation, Writing − original draft. **Nisa Demirbilek:** Formal analysis, Investigation, Writing − original draft. **Lokman Liv:** Methodology, Formal analysis, Investigation, Writing − original draft.

Declaration of competing interest

The authors declare that they have no known competing financial interests or personal relationships that could have appeared to influence the work reported in this paper.

Acknowledgements

The authors gratefully acknowledge TUBITAK UME for financial support and thank to Özgür Duygulu at TUBITAK MAM-Materials Institute for TEM experiments.

Appendix A. Supplementary data

Supplementary data to this article can be found online at https://doi.org/10.1016/j.aca.2021.338939.

References

[1] C. Sohrabi, Z. Alsafi, N. O'Neill, M. Khan, A. Kerwan, A. Al-Jabir, C. Iosifidis, R. Agha, World Health Organization declares global emergency, A review of the 2019 novel coronavirus (COVID-19), Int. J. Surg. 76 (2020) 71−76.
[2] F. Wu, S. Zhao, B. Yu, Y.-M. Chen, W. Wang, Z.-G. Song, Y. Hu, Z.-W. Tao, J.-H. Tian, Y.-Y. Pei, M.-L. Yuan, Y.-L. Zhang, F.-H. Dai, Y. Liu, Q.-M. Wang, J.-J. Zheng, L. Xu, E.C. Holmes, Y.-Z. Zhang, A new coronavirus associated with human respiratory disease in China, Nature 579 (2020) 265−269.
[3] N. Zhu, D. Zhang, W. Wang, X. Li, B. Yang, J. Song, X. Zhao, B. Huang, W. Shi, R. Lu, P. Niu, F. Zhan, X. Ma, D. Wang, W. Xu, G. Wu, G.F. Gao, W. Tan, A novel coronavirus from patients with pneumonia in China, 2019, N. Engl. J. Med. 382 (2020) 727−733.
[4] C. Wang, P.W. Horby, F.G. Hayden, G.F. Gao, A novel coronavirus outbreak of global health concern, Lancet 395 (2020) 470−473.
[5] C. Huang, Y. Wang, X. Li, L. Ren, J. Zhao, Y. Hu, L. Zhang, G. Fan, J. Xu, X. Gu, Z. Cheng, T. Yu, J. Xia, Y. Wei, W. Wu, X. Xie, W. Yin, H. Li, M. Liu, Y. Xiao, H. Gao, L. Guo, J. Xie, G. Wang, R. Jiang, Z. Gao, Q. Jin, J. Wang, B. Cao, Clinical features of patients infected with 2019 novel coronavirus in Wuhan, China, Lancet 395 (2020) 497−506.
[6] D. Baud, X. Qi, K. Nielsen-Saines, D. Musso, L. Pomar, G. Favre, Real estimates of mortality following COVID-19 infection, Lancet Infect. Dis. 20 (2020) 773.
[7] D. Wang, B. Hu, C. Hu, F. Zhu, X. Liu, J. Zhang, B. Wang, H. Xiang, Z. Cheng, Y. Xiong, Y. Zhao, Y. Li, X. Wang, Z. Peng, Clinical characteristics of 138 hospitalized patients with 2019 novel coronavirus−infected pneumonia in wuhan, China, J. Am. Med. Assoc. 323 (2020) 1061−1069.
[8] N. Chen, M. Zhou, X. Dong, J. Qu, F. Gong, Y. Han, Y. Qiu, J. Wang, Y. Liu, Y. Wei, J. Xia, T. Yu, X. Zhang, L. Zhang, Epidemiological and clinical characteristics of 99 cases of 2019 novel coronavirus pneumonia in Wuhan, China: a descriptive study, Lancet 395 (2020).
[9] J. Chan, S. Yuan, K.-H. Kok, K. To, H. Chu, J. Yang, F. Xing, J. Liu, C. Yip, R. Poon, H.-W. Tsoi, S. Lo, K.-H. Chan, V. Poon, W.-M. Chan, J. Ip, J.-P. Cai, V. Cheng, H. Chen, K.-Y. Yuen, A familial cluster of pneumonia associated with the 2019 novel coronavirus indicating person-to-person transmission: a study of a family cluster, Lancet 395 (2020).
[10] P. Yu, J. Zhu, Z. Zhang, Y. Han, A familial cluster of infection associated with the 2019 novel coronavirus indicating possible person-to-person transmission during the incubation period, J. Infect. Dis. 221 (2020) 1757−1761.
[11] P. Pokhrel, C. Hu, H. Mao, Detecting the coronavirus (COVID-19), ACS Sens. 5 (2020) 2283−2296.
[12] B. Udugama, P. Kadhiresan, H.N. Kozlowski, A. Malekjahani, M. Osborne, V.Y.C. Li, H. Chen, S. Mubareka, J.B. Gubbay, W.C.W. Chan, Diagnosing COVID-19: the disease and tools for detection, ACS Nano 14 (2020) 3822−3835.
[13] S. Iravani, Nano- and biosensors for the detection of SARS-CoV-2: challenges and opportunities, Mater. Adv. 1 (2020) 3092−3103.
[14] H. Maddali, C.E. Miles, J. Kohn, D.M. O'Carroll, Optical biosensors for virus detection: prospects for SARS-CoV-2/COVID-19, Chembiochem 22 (2021) 1176−1189.
[15] D. Schoeman, B.C. Fielding, Coronavirus envelope protein: current knowledge, Virol. J. 16 (2019) 69.
[16] W. Hu, L. Zeng, S. Zhai, C. Li, W. Feng, Y. Feng, Z. Liu, Developing a ratiometric two-photon probe with baseline resolved emissions by through band energy transfer strategy: tracking mitochondrial SO_2 during neuroinflammation, Biomaterials 241 (2020) 119910.
[17] K. Kuba, Y. Imai, S. Rao, H. Gao, F. Guo, B. Guan, Y. Huan, P. Yang, Y. Zhang, W. Deng, L. Bao, B. Zhang, G. Liu, Z. Wang, M. Chappell, Y. Liu, D. Zheng, A. Leibbrandt, T. Wada, A.S. Slutsky, D. Liu, C. Qin, C. Jiang, J.M. Penninger, A crucial role of angiotensin converting enzyme 2 (ACE2) in SARS

coronavirus—induced lung injury, Nat. Med. 11 (2005) 875—879.
[18] R. Lu, X. Zhao, J. Li, P. Niu, B. Yang, H. Wu, W. Wang, H. Song, B. Huang, N. Zhu, Y. Bi, X. Ma, F. Zhan, L. Wang, T. Hu, H. Zhou, Z. Hu, W. Zhou, L. Zhao, J. Chen, Y. Meng, J. Wang, Y. Lin, J. Yuan, Z. Xie, J. Ma, W.J. Liu, D. Wang, W. Xu, E.C. Holmes, G.F. Gao, G. Wu, W. Chen, W. Shi, W. Tan, Genomic characterisation and epidemiology of 2019 novel coronavirus: implications for virus origins and receptor binding, Lancet 395 (2020) 565—574.
[19] F. Krammer, V. Simon, Serology assays to manage COVID-19, Science 368 (2020) 1060—1061.
[20] X. Ou, Y. Liu, X. Lei, P. Li, D. Mi, L. Ren, L. Guo, R. Guo, T. Chen, J. Hu, Z. Xiang, Z. Mu, X. Chen, J. Chen, K. Hu, Q. Jin, J. Wang, Z. Qian, Characterization of spike glycoprotein of SARS-CoV-2 on virus entry and its immune cross-reactivity with SARS-CoV, Nat. Commun. 11 (2020) 1620.
[21] L. Lan, D. Xu, G. Ye, C. Xia, S. Wang, Y. Li, H. Xu, Positive RT-PCR test results in patients recovered from COVID-19, J. Am. Med. Assoc. 323 (2020) 1502—1503.
[22] J.F.-W. Chan, C.C.-Y. Yip, K.K.-W. To, T.H.-C. Tang, S.C.-Y. Wong, K.-H. Leung, A.Y.-F. Fung, A.C.-K. Ng, Z. Zou, H.-W. Tsoi, G.K.-Y. Choi, A.R. Tam, V.C.-C. Cheng, K.-H. Chan, O.T.-Y. Tsang, K.-Y. Yuen, Improved molecular diagnosis of COVID-19 by the novel, highly sensitive and specific COVID-19-RdRp/Hel real-time reverse transcription-PCR assay validated in vitro and with clinical specimens, J. Clin. Microbiol. 58 (2020) 10—20.
[23] Y. Li, L. Yao, J. Li, L. Chen, Y. Song, Z. Cai, C. Yang, Stability issues of RT-PCR testing of SARS-CoV-2 for hospitalized patients clinically diagnosed with COVID-19, J. Med. Virol. 92 (2020) 903—908.
[24] Y. Fang, H. Zhang, J. Xie, M. Lin, L. Ying, P. Pang, W. Ji, Sensitivity of chest CT for COVID-19: comparison to RT-PCR, Radiology 296 (2020). E115—E117.
[25] E. Adams, M. Ainsworth, R. Anand, M.I. Andersson, K. Auckland, J.K. Baillie, E. Barnes, S. Beer, J.I. Bell, T. Berry, S. Bibi, M. Carroll, S.K. Chinnakannan, E. Clutterbuck, R.J. Cornall, D.W. Crook, T. de Silva, W. Dejnirattisai, K.E. Dingle, C. Dold, A. Espinosa, D.W. Eyre, H. Farmer, M.F. Mendoza, D. Georgiou, S.J. Hoosdally, A. Hunter, K. Jeffrey, P. Klenerman, J. Knight, C. Knowles, A.J. Kwok, U. Leuschner, R. Levin, C. Liu, C. López-Camacho, J. Martinez, P.C. Matthews, H. McGivern, A.J. Mentzer, J. Milton, J. Mongkolsapaya, S.C. Moore, M.S. Oliveira, F. Pereira, E. Perez, T. Peto, R.J. Ploeg, A. Pollard, T. Prince, D.J. Roberts, J.K. Rudkin, V. Sanchez, G.R. Screaton, M.G. Semple, D.T. Skelly, E.N. Smith, A. Sobrinodiaz, J. Staves, D.I. Stuart, P. Supasa, T. Surik, H. Thraves, P. Tsang, L. Turtle, A.S. Walker, B. Wang, C. Washington, N. Watkins, J. Whitehouse, Evaluation of antibody testing for SARS-CoV-2 using ELISA and lateral flow immunoassays, Wellcome Open Res. 5 (2020).
[26] P. Brangel, A. Sobarzo, C. Parolo, B.S. Miller, P.D. Howes, S. Gelkop, J.J. Lutwama, J.M. Dye, R.A. McKendry, L. Lobel, M.M. Stevens, A serological point-of-care test for the detection of IgG antibodies against ebola virus in human survivors, ACS Nano 12 (2018) 63—73.
[27] X. Li, Q. Zhang, P. Hou, M. Chen, W. Hui, A. Vermorken, Z. Luo, H. Li, Q. Li, Y. Cui, Gold magnetic nanoparticle conjugate-based lateral flow assay for the detection of IgM class antibodies related to TORCH infections, Int. J. Mol. Med. 36 (2015) 1319—1326.
[28] T. Wen, C. Huang, F.-J. Shi, X.-Y. Zeng, T. Lu, S.-N. Ding, Y.-J. Jiao, Development of a lateral flow immunoassay strip for rapid detection of IgG antibody against SARS-CoV-2 virus, Analyst 145 (2020) 5345—5352.
[29] B.E. Fan, V.C.L. Chong, S.S.W. Chan, G.H. Lim, K.G.E. Lim, G.B. Tan, S.S. Mucheli, P. Kuperan, K.H. Ong, Hematologic parameters in patients with COVID-19 infection, Am. J. Hematol. 95 (2020). E131—E134.
[30] Y.-W. Tang, J.E. Schmitz, D.H. Persing, C.W. Stratton, Laboratory diagnosis of COVID-19: current issues and challenges, J. Clin. Microbiol. 58 (2020) 12—20.
[31] M.J. Marín, A. Rashid, M. Rejzek, S.A. Fairhurst, S.A. Wharton, S.R. Martin, J.W. McCauley, T. Wileman, R.A. Field, D.A. Russell, Glyconanoparticles for the plasmonic detection and discrimination between human and avian influenza virus, Org. Biomol. Chem. 11 (2013) 7101—7107.
[32] C. Lee, M. Gaston, A. Weiss, P. Zhang, Colorimetric viral detection based on sialic acid stabilized gold nanoparticles, Biosens. Bioelectron. 42 (2013) 236—241.
[33] Y. Liu, L. Zhang, W. Wei, H. Zhao, Z. Zhou, Y. Zhang, S. Liu, Colorimetric detection of influenza A virus using antibody-functionalized gold nanoparticles, Analyst 140 (2015) 3989—3995.
[34] C.R. Basso, C.C. Tozato, B.P. Crulhas, G.R. Castro, J.P.A. Junior, V.A. Pedrosa, An easy way to detect dengue virus using nanoparticle-antibody conjugates, Virology 513 (2018) 85—90.
[35] S.Y. Yi, U. Lee, B.H. Chung, J. Jung, A scanometric antibody probe for facile and sensitive immunoassays, Chem. Commun. 51 (2015) 8865—8867.
[36] E. Cesewski, B.N. Johnson, Electrochemical biosensors for pathogen detection, Biosens. Bioelectron. 159 (2020) 112214.
[37] R. Wang, C. Xue, M. Gao, H. Qi, C. Zhang, Ultratrace voltammetric method for the detection of DNA sequence related to human immunodeficiency virus type 1, Microchim. Acta. 172 (2011) 291—297.
[38] F. Walters, S. Rozhko, D. Buckley, E.D. Ahmadi, M.M. Ali, Z. Tehrani, J.J. Mitchell, G. Burwell, Y. Liu, O. Kazakova, O.J. Guy, Real-time detection of hepatitis B surface antigen using a hybrid graphene-gold nanoparticle biosensor, 2D Mater. 7 (2020), 024009.
[39] B.S.S. Guirgis, C. Sá e Cunha, I. Gomes, M. Cavadas, I. Silva, G. Doria, G.L. Blatch, P. V Baptista, E. Pereira, H.M.E. Azzazy, M.M. Mota, M. Prudêncio, R. Franco, Gold nanoparticle-based fluorescence immunoassay for malaria antigen detection, Anal. Bioanal. Chem. 402 (2012) 1019—1027.
[40] C. Ménard-Moyon, A. Bianco, K. Kalantar-Zadeh, Two-dimensional material-based biosensors for virus detection, ACS Sens. 5 (2020) 3739—3769.
[41] K. Dziąbowska, E. Czaczyk, D. Nidzworski, Detection methods of human and animal influenza virus—current trends, Biosensors 8 (2018) 94.
[42] B.V. Ribeiro, T.A.R. Cordeiro, G.R. Oliveira e Freitas, L.F. Ferreira, D.L. Franco, Biosensors for the detection of respiratory viruses: a review, Talanta Open 2 (2020) 100007.
[43] M.S. Draz, H. Shafiee, Applications of gold nanoparticles in virus detection, Theranostics 8 (2018) 1985—2017.
[44] C.-C. Chang, C.-P. Chen, T.-H. Wu, C.-H. Yang, C.-W. Lin, C.-Y. Chen, Gold nanoparticle-based colorimetric strategies for chemical and biological sensing applications, Nanomaterials 9 (2019) 861.
[45] M.H. Jazayeri, T. Aghaie, A. Avan, A. Vatankhah, M.R.S. Ghaffari, Colorimetric detection based on gold nano particles (GNPs): an easy, fast, inexpensive, low-cost and short time method in detection of analytes (protein, DNA, and ion), Sens. Bio-Sensing Res. 20 (2018) 1—8.
[46] H. Aldewachi, T. Chalati, M.N. Woodroofe, N. Bricklebank, B. Sharrack, P. Gardiner, Gold nanoparticle-based colorimetric biosensors, Nanoscale 10 (2018) 18—33.
[47] J.P. Oliveira, A.R. Prado, W.J. Keijok, P.W.P. Antunes, E.R. Yapuchura, M.C.C. Guimarães, Impact of conjugation strategies for targeting of antibodies in gold nanoparticles for ultrasensitive detection of 17β-estradiol, Sci. Rep. 9 (2019) 13859.
[48] L. Zhang, Y. Mazouzi, M. Salmain, B. Liedberg, S. Boujday, Antibody-gold nanoparticle bioconjugates for biosensors: synthesis, characterization and selected applications, Biosens. Bioelectron. 165 (2020) 112370.
[49] M.H. Jazayeri, H. Amani, A.A. Pourfatollah, H. Pazoki-Toroudi, B. Sedighimoghaddam, Various methods of gold nanoparticles (GNPs) conjugation to antibodies, Sens. Bio-Sensing Res. 9 (2016) 17—22.
[50] M.S. Khan, S.K. Misra, K. Dighe, Z. Wang, A.S. Schwartz-Duval, D. Sar, D. Pan, Electrically-receptive and thermally-responsive paper-based sensor chip for rapid detection of bacterial cells, Biosens. Bioelectron. 110 (2018) 132—140.
[51] M.S. Khan, K. Dighe, Z. Wang, I. Srivastava, A.S. Schwartz-Duval, S.K. Misra, D. Pan, Electrochemical-digital immunosensor with enhanced sensitivity for detecting human salivary glucocorticoid hormone, Analyst 144 (2019) 1448—1457.
[52] F. Liu, K.S. Choi, T.J. Park, S.Y. Lee, T.S. Seo, Graphene-based electrochemical biosensor for pathogenic virus detection, BioChip J 5 (2011) 123—128.
[53] L.A. Layqah, S. Eissa, An electrochemical immunosensor for the corona virus associated with the Middle East respiratory syndrome using an array of gold nanoparticle-modified carbon electrodes, Microchim. Acta. 186 (2019) 224.
[54] B. Della Ventura, M. Cennamo, A. Minopoli, R. Campanile, S. Bolletti Censi, D. Terracciano, G. Portella, R. Velotta, Colorimetric test for fast detection of SARS-CoV-2 in nasal and throat swabs, ACS Sens. 5 (2020) 3043—3048.
[55] P. Moitra, M. Alafeef, K. Dighe, M.B. Frieman, D. Pan, Selective naked-eye detection of SARS-CoV-2 mediated by N gene targeted antisense oligonucleotide capped plasmonic nanoparticles, ACS Nano 14 (2020) 7617—7627.
[56] B. Vadlamani, T. Uppal, S. Verma, M. Misra, Functionalized TiO_2 nanotube-based electrochemical biosensor for rapid detection of SARS-CoV-2, Sensors 20 (2020) 5871.
[57] R. Torrente-Rodríguez, H. Lukas, J. Tu, J. Min, Y. Yang, C. Xu, H. Rossiter, W. Gao, SARS-CoV-2 RapidPlex, A graphene-based multiplexed telemedicine platform for rapid and low-cost COVID-19 diagnosis and monitoring, Matter 3 (2020) 1981—1998.
[58] H. Zhao, F. Liu, W. Xie, T.-C. Zhou, J. OuYang, L. Jin, H. Li, C.-Y. Zhao, L. Zhang, J. Wei, Y.-P. Zhang, C.-P. Li, Ultrasensitive super sandwich-type electrochemical sensor for SARS-CoV-2 from the infected COVID-19 patients using a smartphone, Sensor. Actuator. B Chem. 327 (2021) 128899.
[59] R. Funari, K.-Y. Chu, A.Q. Shen, Detection of antibodies against SARS-CoV-2 spike protein by gold nanospikes in an opto-microfluidic chip, Biosens. Bioelectron. 169 (2020) 112578.
[60] A. Ahmadivand, B. Gerislioglu, Z. Ramezani, A. Kaushik, P. Manickam, S.A. Ghoreishi, Functionalized terahertz plasmonic metasensors: femtomolar-level detection of SARS-CoV-2 spike proteins, Biosens. Bioelectron. 177 (2021) 112971.
[61] L. Huang, L. Ding, J. Zhou, S. Chen, F. Chen, C. Zhao, J. Xu, W. Hu, J. Ji, H. Xu, G.L. Liu, One-step rapid quantification of SARS-CoV-2 virus particles via low-cost nanoplasmonic sensors in generic microplate reader and point-of-care device, Biosens. Bioelectron. 171 (2021) 112685.
[62] A. Pramanik, Y. Gao, S. Patibandla, D. Mitra, M.G. McCandless, L.A. Fassero, K. Gates, R. Tandon, P. Chandra Ray, The rapid diagnosis and effective inhibition of coronavirus using spike antibody attached gold nanoparticles, Nanoscale Adv. 3 (2021) 1588—1596.
[63] G. Seo, G. Lee, M.J. Kim, S.-H. Baek, M. Choi, K.B. Ku, C.-S. Lee, S. Jun, D. Park, H.G. Kim, S.-J. Kim, J.-O. Lee, B.T. Kim, E.C. Park, S. Il Kim, Rapid detection of COVID-19 causative virus (SARS-CoV-2) in human nasopharyngeal swab specimens using field-effect transistor-based biosensor, ACS Nano 14 (2020) 5135—5142.
[64] M. Alafeef, K. Dighe, P. Moitra, D. Pan, Rapid, ultrasensitive, and quantitative detection of SARS-CoV-2 using antisense oligonucleotides directed electrochemical biosensor chip, ACS Nano 14 (2020) 17028—17045.
[65] C. Huang, T. Wen, F.-J. Shi, X.-Y. Zeng, Y.-J. Jiao, Rapid detection of IgM antibodies against the SARS-CoV-2 virus via colloidal gold nanoparticle-based lateral-flow assay, ACS Omega 5 (2020) 12550—12556.
[66] L. Fabiani, M. Saroglia, G. Galatà, R. De Santis, S. Fillo, V. Luca, G. Faggioni, N. D'Amore, E. Regalbuto, P. Salvatori, G. Terova, D. Moscone, F. Lista, F. Arduini, Magnetic beads combined with carbon black-based screen-printed

electrodes for COVID-19: a reliable and miniaturized electrochemical immunosensor for SARS-CoV-2 detection in saliva, Biosens. Bioelectron. 171 (2021) 112686.
[67] L. Liv, Electrochemical immunosensor platform based on gold-clusters, cysteamine and glutaraldehyde modified electrode for diagnosing COVID-19, Microchem. J. 168 (2021) 106445.
[68] L. Liv, G. Çoban, N. Nakiboğlu, T. Kocagöz, A rapid, ultrasensitive voltammetric biosensor for determining SARS-CoV-2 spike protein in real samples, Biosens. Bioelectron. 192 (2021) 113497.
[69] B. V Enustun, J. Turkevich, Coagulation of colloidal gold, J. Am. Chem. Soc. 85 (1963) 3317–3328.
[70] S. Lou, J. Ye, K. Li, A. Wu, A gold nanoparticle-based immunochromatographic assay: the influence of nanoparticulate size, Analyst 137 (2012) 1174–1181.